Friulian Journal of Science **30.** 2020, 21-35

Identification of concentrated masses in nanoresonators

MICHELE DILENA*, MARTA FEDELE DELL'OSTE*,
JOSÉ FERNÁNDEZ-SÁEZ**,
ANTONINO MORASSI* & RAMÓN ZAERA**

Abstract. In this paper we review some recent results concerning inverse problems of mass detection in nanobeams by resonant frequency measurements. The nanobeam is modelled within the modified strain gradient theory, according to the Euler-Bernoulli kinematic assumptions. We first consider the identification of a single small point mass in a uniform nanobeam supported at the ends. By linearizing the inverse problem near the referential system, it turns out that knowledge of the shifts in the first two resonant frequencies allows for the unique determination of the mass intensity and the mass position, up to a symmetrical position. Closed form expressions are derived for the position and the intensity of the added mass. In the second part of the paper, the method is extended to the identification of two small point masses added in a supported uniform nanobeam by using the shifts in the first four resonant frequencies.

Key-words. Nanoresonator sensors, point masses, identification, inverse problems.

1. Introduction. Nanosensors are gathering attention in the last years due to the necessity of measuring physical and chemical properties in industrial or biological systems in the sub-micron scale. The reduced dimensions of these transducers lead to novel sensing concepts and to

* Polytechnic Department of Engineering and Architecture, University of Udine, Via Cotonificio 114, 33100 Udine, Italy. E-mail: antonino.morassi@uniud.it
** Department of Continuum Mechanics and Structural Analysis, Universidad Carlos III de Madrid, Av. de la Universidad 30, 28911 Legan es, Madrid, Spain.

an enhanced performance with a great impact on a diversity of applications (Voiculescu and Zaghloul, 2015; Lim, 2011). One of the most representative examples of the advantages of down-scaling in sensoring systems is the nanomechanical resonator, which consists in a vibrating structure with remarkable performance in detecting small adherent masses which produce slight changes in the resonant frequencies of the system (Wang and Arash, 2014). The *mass sensing principle* for these systems is based on using the resonant frequency shifts caused by unknown additional masses attached on the surface of the sensor as data for reconstructing the mass variation.

Derived from atomic force microscopy techniques, the nanobeam-based sensor is one of the most common system used for mass detection. From its beginnings, nanobeams have been used for the detection of micro-sized particles (Braun et al., 2005), cells and fungal spores (Gfeller et al., 2005), DNA molecules (Datar et al., 2009), and even atoms (Jensen et al., 2008). Some recent studies have investigated the suitability of $2D$ resonators, such as nanomembranes and nanoplates, for sensing uses, see, for instance, Alava et al. (2010), Bhaswara et al. (2014) and Fernández-Sáez et al. (2019).

A key feature of the nanostructures is the need of considering size effects when modelling their mechanical response, since their dimensions become comparable to the characteristic microstructural distances. To that aim, generalized continuum models succeed in capturing the effects of microstructure and size effects (Kröner, 1963; Toupin, 1963; Green and Rivlin, 1964; Mindlin, 1964). Among the various strain gradient theories, the one proposed in Lam et al. (2003) (known as *modified strain gradient theory*) arises as an attractive alternative to overcome the difficulties associated with the fully nonlocal elasticity framework, see Romano et al. (2017), and has been used by different authors to analyse the mechanical response of different kind of nanostructures.

In spite of important applications in physical, chemical and biological fields, few theoretical investigations on the inverse problem of detecting added mass in nanoresonators are available. Using the modified strain gradient theory, Morassi et al. (2017) analysed for the first time the axial vibration of a uniform nanorod with a single attached mass of small magnitude, and proposed an identification method for determining mass intensity and position based on an eigenvalue perturbation approach. The above results were extended in Morassi et al. (2019) to the bending vibration of uniform nanobeams with a small attached point mass. Basing on the explicit expression of the first-order eigenfrequency change induced by the point mass, closed-form expression of both the location and the intensity of the point mass were obtained for supported end conditions.

In Sections 2 and 3 of this note we review some of the results obtained in Morassi et al. (2019). In Section 4, we generalize the analysis to the identification of two small point masses in a uniform supported nanobeam from minimal resonant frequency data.

2. Identification of a small point mass in a nanobeam by two resonant frequencies. We shall introduce our inverse problem in mathematical terms. Assuming the kinematic hypotheses of the Euler-Bernoulli's beam theory and working within the modified strain gradient theory proposed by Kong et al. (2009), the spatial amplitude $u = u(x)$ of the free transverse vibration with radian frequency $\sqrt{\lambda}$ of the referential uniform nanobeam is governed by the equation

$$Su^{IV} - KU^{VI} = \lambda \rho u, \quad \text{in } (0, L), \tag{2.1}$$

where L is the length of the nanobeam and ρ is the mass per unit length. The coefficients S and K are given by

$$S = EI + 2GAl_0^2 + \frac{120}{225}GAl_1^2 + GAl_2^2, \quad K = I\left(2Gl_0^2 + \frac{4}{5}Gl_1^2\right), \tag{2.2}$$

where G is the shear modulus, E the Young's modulus, I the second moment of the area, ν the Poisson ratio, and l_0, l_1, l_2 are the additional material constants needed to complete the model; see (Akgoz and Civalek, 2011). Note that when $l_i = 0$, $i = 0, 1, 2$, this formulation coincides with the classical one.

In this paper we will be concerned with supported nanobeams, namely, the following boundary conditions hold at both ends $x = 0$, $x = L$:

$$u(x) = 0, \quad -Su''(x) + Ku^{IV}(x) = 0, \quad u''(x) = 0. \tag{2.3}$$

The eigenpairs of (2.1), (2.3) have the following closed-form expression:

$$\lambda_n = \left(\frac{n\pi}{L}\right)^6 \left[\frac{K}{\rho} + \frac{S}{\rho}\frac{1}{\left(\frac{n\pi}{L}\right)^2}\right], \tag{2.4}$$

$$u_n(x) = \sqrt{\frac{2}{\rho L}} \sin\left(\frac{n\pi x}{L}\right), \quad n \geq 1. \tag{2.5}$$

Suppose that the nanobeam is carrying an attached point mass of intensity $M > 0$ at the point of abscissa $x = s$, $0 < s < L$. The corresponding *perturbed* eigenvalue problem consists in determining the eigenpair $\{\widetilde{\lambda}, \widetilde{u}(x)\}$ solution to

$$\begin{cases} S\widetilde{u}^{IV} - K\widetilde{u}^{VI} = \widetilde{\lambda}\rho\widetilde{u}, \quad \text{in } (0,s) \cup (s,L), \\ \widetilde{u}(0) = \widetilde{u}''(0) = 0, \\ (-S\widetilde{u}'' + K\widetilde{u}^{IV})(0) = 0, \\ [[\widetilde{u}(s)]] = 0, \\ [[\widetilde{u}'(s)]] = 0, \\ [[\widetilde{u}''(s)]] = 0, \\ [[(-S\widetilde{u}''' + K\widetilde{u}^{V})(s)]] = -\widetilde{\lambda}M\widetilde{u}(s), \\ [[(-S\widetilde{u}'' + K\widetilde{u}^{IV})(s)]] = 0, \\ [[K\widetilde{u}'''(s)]] = 0, \\ (-S\widetilde{u}'' + K\widetilde{u}^{IV})(L) = 0, \\ \widetilde{u}(L) = \widetilde{u}''(L) = 0. \end{cases} \tag{2.6}$$

Here, $[[f(s)]] \equiv (f(s^+) - f(s^-)) = \lim_{x\to s^+} f(x) - \lim_{x\to s^-} f(x)$.

Let us assume that the added mass is small with respect to the total mass of the nanobeam, e.g., $M << \rho L$. By classical results, it turns out that the nth eigenvalue $\widetilde{\lambda}_n = \widetilde{\lambda}_n(M)$ is a C^1-function in $[0,\infty)$ of the mass M, and the first derivative has the explicit expression

$$\frac{\partial\widetilde{\lambda}_n}{\partial M} = -\widetilde{\lambda}_n \frac{\widetilde{u}_n^2(s)}{M\widetilde{u}_n^2(s) + \int_0^L \rho\widetilde{u}_n^2}. \tag{2.7}$$

By (2.7), the first-order approximation of the nth perturbed eigenvalue with respect to M is

$$\widetilde{\lambda}_n(M) = \lambda_n - \lambda_n u_n^2(s) M, \tag{2.8}$$

where the mass-normalization condition $\int_0^L \rho u_n^2 = 1$ has been taken into account. By substituting the expressions (2.4), (2.5) in (2.8) we obtain

$$C_n^S = M \sin^2\left(\frac{n\pi s}{L}\right), \tag{2.9}$$

with

$$C_n^S = -\frac{\left(\widetilde{\lambda}_n - \lambda_n\right)}{\lambda_n}\frac{\rho L}{2}, \quad n \geq 1. \tag{2.10}$$

The expression (2.9) shows that the identification of the point mass can be performed by using a specific pair of resonant frequency shifts, namely those corresponding to the nth and $2n$th eigenfrequencies, for $n \geq 1$. In fact, if $C_n^S > 0$, then the following closed-form expressions for mass intensity and position can be derived:

$$M = \frac{C_n^S}{1 - \frac{C_{2n}^S}{4C_n^S}}, \tag{2.11}$$

$$\cos\left(\frac{2n\pi s}{L}\right) = \frac{C_{2n}^S}{2C_n^S} - 1. \tag{2.12}$$

Conversely, if $C_n^S = 0$ for certain $n \geq 2$, then the point mass is located in one of the nodal points of the nth vibration mode. The mass intensity remains undetermined in this case.

Finally, it is worth noting that the measurement of the first two resonant frequency shifts determines uniquely the position of the point mass up to symmetry with respect to $x = L/2$.

3. Applications. In this section we shall evaluate the accuracy of the perturbation approach in estimating the first two natural frequencies of the supported nanobeam. Moreover, we shall apply the above resonant-based detection method with $n = 1$ to identify both position and intensity of the point mass.

For illustration purposes, material and geometrical properties of the nanobeam are taken as in Kong et al. (2009). The nanobeam is assumed to have an equivalent rectangular cross-section, with thickness $h = 50$ μm, width $b = 2h$, length $L = 20h$, Young's modulus $E = 1.44$ GPa, and Poisson ratio $\nu = 0.38$. The three length scale parameters are assumed to be equal, e.g., $l_i = 17.6$ μm, $i = 0, 1, 2$.

The accuracy of the perturbation approach is tested by comparing the values of the eigenfrequencies determined by solving exactly the problem (2.6) and their approximate values obtained via the perturbative solution (2.8). The results for different values of h/l and for different positions s/L of the point mass (normalized to the total mass ρL) are plotted in Figures 1 and 2. Numerical results show that the accuracy of

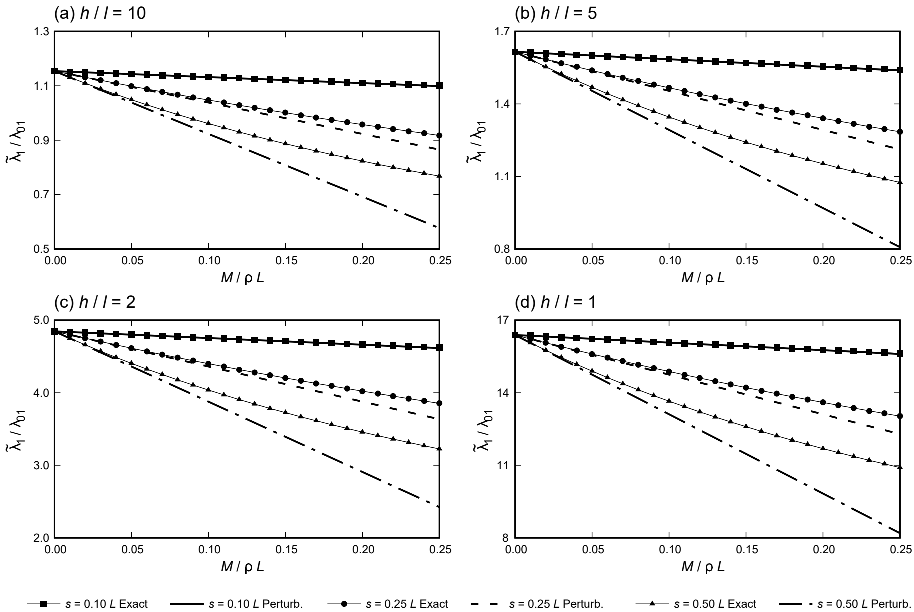

Figure 1: Normalized first eigenvalue versus dimensionless point-mass, for different mass position and different values of length scale parameter.

the perturbative frequency estimate is rather uniform with respect to the scale factor l, at least in the range of values considered. Typically, the smaller the amplitude $u_n(s)$, the better the accuracy. In particular, the maximum difference between exact and first-order resonant frequency value is encountered at $s/L = 0.50$ and $s/L = 0.25$ for the first and second mode, respectively. Maximum deviations are about 1, 4, 9 % (first mode) and 1, 5, 11 % (second mode) for $M/(\rho L) = 0.05, 0.10, 0.15$, respectively.

In applying the identification method, frequency shifts have been evaluated by solving exactly the direct eigenvalue problem in referential and perturbed configuration. The simulations have been performed with noise-free data, although an intrinsic approximation is still present due to the first-order truncation (2.8) in the Taylor series of the eigenvalues. Figure 3 shows the results varying continuously the position s/L of

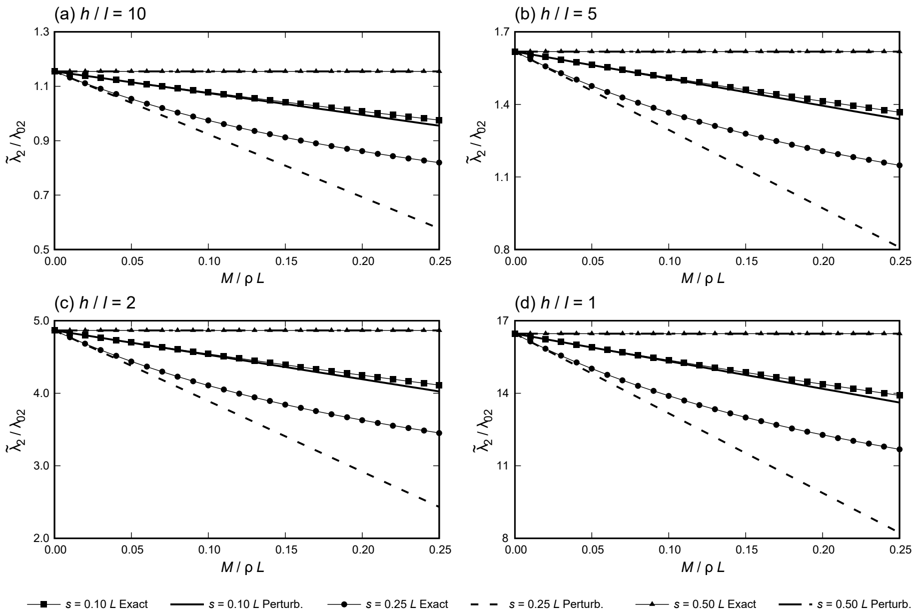

Figure 2: Normalized second eigenvalue versus dimensionless point-mass, for different mass position and different values of length scale parameter.

the point mass within the interval $[0, 1/2]$ and using selected values of the normalized mass intensity $M/(\rho L) = 0.010, 0.025, 0.050, 0.100, 0.150, 0.200$. These values correspond approximately to maximum relative shifts $\delta\lambda_n/\lambda_n$ equal to $2, 5, 9, 17, 23, 29\%$ and $2, 5, 9, 16, 22, 26\%$ for $n = 1$ and $n = 2$, respectively. The maximum error on the mass position is about 5% for $M/(\rho L) = 0.200$, and estimates remain accurate even for high mass values. The determination of the mass intensity is less accurate, with errors up to $15 - 30\%$ and $40 - 50\%$ for $M/(\rho L) = 0.050 - 0.100$ and $M/(\rho L) = 0.150 - 0.200$, respectively.

4. Identification of two point masses. The analysis developed in the above section can be extended to the identification of two small point masses (s_1, M_1), (s_2, M_2) attached on a uniform supported nanobeam from the changes in the first four resonant frequencies, where $0 < s_1 < s_2 < L$ and $M_i << \rho L$, $i = 1, 2$.

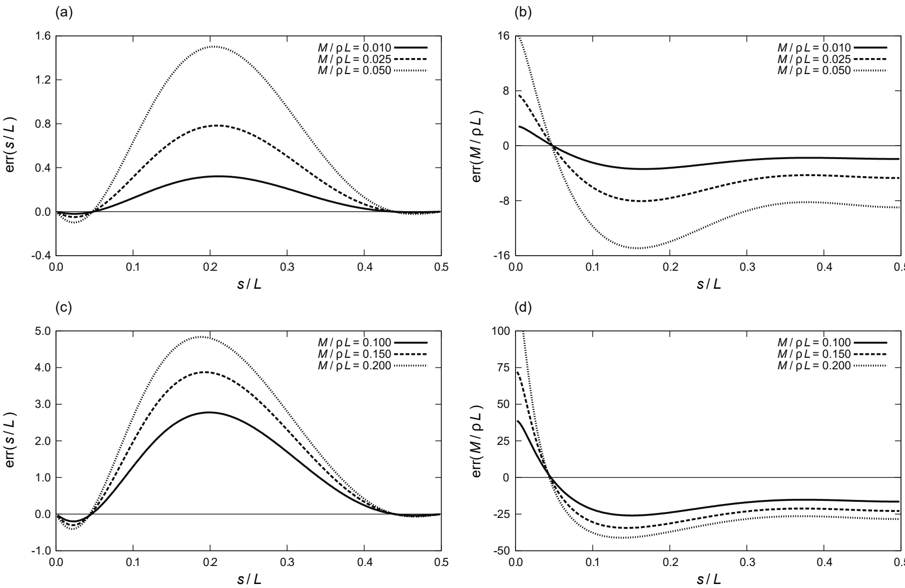

Figure 3: Identification using the variations of the first two eigenfrequencies for different values of the point-mass. Left column: percentage errors on the mass position, $err(s) = 100 \times (s_{ident} - s_{exact})/L$. Right column: percentage errors on the mass intensity, $err(M/(\rho L)) = 100 \times (M_{ident} - M_{exact})/M_{exact}$.

The undamped free transverse vibrations of the perturbed nanobeam satisfy the boundary value problem (2.6), in which the differential equation holds in $(0, s_1) \cup (s_1, s_2) \cup (s_2, L)$ and the jump conditions hold at the cross-sections $x = s_1$ and $x = s_2$. On proceeding as in Section 2 and with the above notation, the first order change of the nth eigenvalue is given by

$$C_n^S = M_1 \sin^2\left(\frac{n\pi s_1}{L}\right) + M_2 \sin^2\left(\frac{n\pi s_2}{L}\right), \tag{4.1}$$

where C_n^S is defined as in (2.10), $n \geq 1$.

By the symmetry of the unperturbed system, the configurations $\{(s_1, M_1), (s_2, M_2)\}$, $\{(L-s_1, M_1), (L-s_2, M_2)\}$, $\{(L-s_1, M_1), (s_2, M_2)\}$, $\{(s_1, M_1), (L-s_2, M_2)\}$ cannot be distinguished from resonant frequency data. Taking into account this intrinsic non-uniqueness of the problem, it is not restrictive to assume

$$0 < s_1 < s_2 \leq \frac{L}{2} \ . \tag{4.2}$$

We now formulate the inverse problem in terms of the changes in the first four natural frequencies. By writing (4.1) for $n = 1, 2, 3, 4$, we obtain the following system of nonlinear equations to be solved with respect to the four parameters (s_1, M_1), (s_2, M_2):

$$\begin{cases} M_1 \sin^2 \frac{\pi s_1}{L} + M_2 \sin^2 \frac{\pi s_2}{L} = C_1^S, \\ M_1 \sin^2 \frac{2\pi s_1}{L} + M_2 \sin^2 \frac{2\pi s_2}{L} = C_2^S, \\ M_1 \sin^2 \frac{3\pi s_1}{L} + M_2 \sin^2 \frac{3\pi s_2}{L} = C_3^S, \\ M_1 \sin^2 \frac{4\pi s_1}{L} + M_2 \sin^2 \frac{4\pi s_2}{L} = C_4^S, \end{cases} \tag{4.3}$$

where

$$C_i^S > 0, \ i = 1, 2, 3, \ C_4^S \geq 0. \tag{4.4}$$

The system (4.3) has the same structure of the system $(13) - (16)$ introduced in Rubio et al. (2016) for the identification of two open cracks of different severity in a (classical) bending beam under simply supported end conditions. Therefore, we can adapt the arguments in Rubio et al. (2016) and find the explicit solution to the nonlinear system (4.3). Omitting the details and referring the interested reader to the above mentioned paper for precise statements, here we recall the main result: the knowledge of the first four natural frequencies allows to uniquely determine the intensity and the location of the two point masses, up to symmetry with respect to the mid-span cross-section. Remarkably, closed-form expressions both for the mass positions and intensities can be obtained in terms of the natural frequency data.

We briefly outline the main arguments that can be used to prove the above result. The particular case in which $C_4^S = 0$ is straightforward. If C_4^S vanishes, then $s_1 = \frac{L}{4}$ and $s_2 = \frac{L}{2}$, and one easily gets

$$M_1 = C_2^S, \quad M_2 = \frac{2C_1^S - C_2^S}{2}. \tag{4.5}$$

In order to discuss the general case, it is convenient to introduce the following *position variables*

$$x = x(s_1) = \cos \frac{2\pi s_1}{L} \in [-1, 1), \quad y = y(s_2) = \cos \frac{2\pi s_2}{L} \in [-1, 1). \tag{4.6}$$

Note that for $s \in (0, L/2]$ the function $f(s) = \cos\left(\frac{2\pi s}{L}\right)$ is a one-to-one correspondence between the interval $(0, L/2]$ and the interval $[-1, 1)$. Therefore, if we are able to find the two variables $\{x, y\}$, then we can determine uniquely the positions $\{s_1, s_2\}$ of the two masses.

Following the arguments show in Rubio et al. (2016), the position variable x turns to be the root of the second order polynomial equation

$$x^2 - Sx + P = 0, \tag{4.7}$$

where the real numbers $S = x + y$ and $P = xy$ can be determined by means of closed-form expressions of the data C_i^S, $i = 1, \dots, 4$. Let us denote by

$$x_\mp = \frac{S \mp \sqrt{S^2 - 4P}}{2} \tag{4.8}$$

the two roots of (4.7), where the notation x_-, x_+ corresponds to $-$ sign and $+$ sign on the right hand side of (4.8), respectively. Moreover, also the position variables y_-, y_+ corresponding to the solution x_-, x_+, respectively, can be determined explicitly. Denoting by (x, y) one of the two solutions (x_-, y_-), (x_+, y_+), the following closed form expressions hold for the mass intensities:

$$M_1 = \frac{C_2 - 2C_1(1 + y)}{(1 - x)(x - y)}, \tag{4.9}$$

$$M_2 = \frac{C_2 - 2C_1(1 + x)}{(1 - y)(y - x)}. \tag{4.10}$$

In conclusion, the complete set of solutions of (4.3) is given by

$$\{(s_{1-}, K_{1-}),\ (s_{2-}, M_{2-})\}, \quad \{(s_{1+}, K_{1+}),\ (s_{2+}, M_{2+})\}, \tag{4.11}$$

where $(M_{1-},\ M_{2-})$, $(M_{1+},\ M_{2+})$ are evaluated by (4.9) with $(x = x_-, y = y_-)$ and by (4.10) with $(x = x_+, y = y_+)$, respectively. The mass positions $s_{i\mp}$, $i = 1, 2$, are obtained by inverting the one-to-one function $\cos\frac{2\pi s}{L}$ on $(0, L/2]$ appearing in (4.6).

Finally, by noticing that $y_- = x_+$, $y_+ = x_-$ and that $M_{1+} = M_{2-}$, $M_{2+} = M_{1-}$, it is easy to show that the two damage configurations (4.11) actually coincide. Therefore, we have shown that the knowledge of the first four natural frequencies allows to determine uniquely the two concentrated masses, up to symmetry with respect to the mid-span cross-section of the nanobeam.

An exhaustive set of numerical simulations has been carried out for different locations of the point masses and various mass intensities. Eight different damage scenarios among several studied are presented and discussed in the sequel: they are illustrative of the main features of the inverse problem and of the identification technique. The first four cases, denoted by a, b, c, d, correspond to the positions $s_1/L = 0.20$, $s_2/L = 0.35$, whereas for the cases e, f, g, h we assumed $s_1/L = 0.20$, $s_2/L = 0.40$. The mass intensities range from 0.4% to 10% of the total mass of the nanobeam, see Table 1.

The eigenvalues of the unperturbed and perturbed system are shown in Table 2. The latter have been obtained by solving exactly the eigenvalue problem with the actual values of the mass parameters. The results of identification are summarized in Table 3. It is possible to observe that the solution predicted by the theory generally is a satisfactory estimate of the actual solution of the inverse problem. The discrepancies between identified and actual mass parameters are exclusively due to the perturbation assumption of small mass. Deviations are typically smaller for masses with small intensity, as it is expected because the inverse problem is linearized in a neighborhood of the unperturbed nanobeam. Maximum errors of about $2 - 3\%$ and $15 - 20\%$ are observed for the position and the intensity, respectively.

For the sake of completeness, we note that numerical simulations have not led to accurate results in the case of close point masses. The motivation of this discrepancy is connected with the reconstruction procedure illustrated above and, specifically, with the determination of the parameters S, P by the inversion of a two-by-two linear system. It can be shown that the inversion of this linear system is ill-posed when $s_1 \simeq s_2$, so that the effects of the assumption of small damage are amplified strongly.

5. Conclusions. The determination of added masses in nanobeams by measurements of resonant frequency shifts is an inverse problem of great relevance and interest in various fields of modern applied sciences. Despite this, theoretical results on this class of problems are still rare. In this note, we review some recent results obtained by the authors in the

Table 1: Two-point mass scenarios $a-h$.

	a	b	c	d	e	f	g	h
s_1/L	0.200	0.200	0.200	0.200	0.200	0.200	0.200	0.200
s_2/L	0.350	0.350	0.350	0.350	0.450	0.450	0.450	0.450
$M_1/(\rho L)$	0.004	0.010	0.040	0.040	0.004	0.010	0.040	0.040
$M_2/(\rho L)$	0.008	0.020	0.050	0.100	0.008	0.020	0.050	0.100

Table 2: First four resonant frequencies f_n^U for the unperturbed nanobeam (U) and their values f_n associated with the eight scenarios $a-h$ of Table 1. Values in Hertz; percentage errors $\Delta = 100 \times (f_n^U - f_n)/f_n^U$ are indicated in brackets.

U	a	b	c	d	e	f	g	h
82226	81597	80679	78146	75467	81480	80399	77514	74350
	(0.76)	(1.88)	(4.96)	(8.22)	(0.91)	(2.22)	(5.73)	(9.58)
329428	326553	322391	308682	301057	327989	325844	316383	314814
	(0.87)	(2.14)	(6.30)	(8.61)	(0.44)	(1.09)	(3.96)	(4.44)
743182	740401	736421	719547	719245	735963	725806	696268	677888
	(0.37)	(0.91)	(3.18)	(3.22)	(0.97)	(2.34)	(6.31)	(8.79)
1326096	1314948	1299229	1259519	1221730	1320697	1312952	1289526	1274119
	(0.84)	(2.03)	(5.02)	(7.87)	(0.41)	(0.99)	(2.76)	(3.92)

Table 3: Results of identification for the eight scenarios $a-h$ of Table 1. Determination of mass intensities M_i and corresponding mass positions s_i, $i = 1, 2$. Percentage errors for position, $err(s) = 100 \times (s_{ident} - s_{exact})/L$, and mass intensity, $err(M) = 100 \times (M_{ident} - M_{exact})/M_{exact}$, are indicated in brackets.

	a	b	c	d	e	f	g	h
s_1/L	0.202	0.206	0.210	0.230	0.202	0.205	0.211	0.223
	(0.24)	(0.59)	(0.96)	(2.96)	(0.21)	(0.51)	(1.14)	(2.30)
s_2/L	0.351	0.352	0.353	0.361	0.449	0.448	0.442	0.443
	(0.08)	(0.21)	(0.30)	(1.10)	(-0.10)	(-0.24)	(-0.83)	(-0.74)
$M_1/(\rho L)$	0.004	0.010	0.037	0.041	0.004	0.010	0.037	0.037
	(4.91)	(3.36)	(-6.44)	(2.80)	(4.13)	(1.52)	(-6.55)	(-8.57)
$M_2/(\rho L)$	0.008	0.020	0.047	0.080	0.008	0.020	0.046	0.084
	(3.64)	(0.12)	(-6.90)	(-20.02)	(3.95)	(0.88)	(-7.25)	(-15.76)

identification of a small concentrated mass in a uniform nanobeam, supported at the ends, by minimal eigenfrequency data. The nanobeam is modelled by the modified strain gradient theory and the identification method is based on a perturbation procedure that exploits the possibility of writing in explicit form the first-order variation of the resonant frequencies induced by a point mass. The method is generalized to the identification of two concentrated masses by measurement of the first four resonant frequencies. Results of numerical simulations are presented to support the predictions of the theory.

References/ Bibliografie

Akgoz B., Civalek O. (2011). Strain gradient elasticity and modified couple stress models for buckling analysis of axially loaded micro-scaled beams. *International Journal of Engineering Science* 49:1268–1280.

Alava T., Mathieu F., Mazenq L., Soyer C., Remiens D., Nicu L. (2010). Silicon-based micromembranes with piezoelectric actuation and piezoresistive detection for sensing purposes in liquid media. *Journal of Micromechanics and Microengineering* 20: article 075014.

Bhaswara A., Keum H., Rhee S., Legrand B., Mathieu F., Kim S., Nicu L., Leichle T. (2014). Fabrication of nanoplate resonating structures via micro-masonry. *Journal of Micromechanics and Microengineering* 24: article 115012.

Braun T., Barwich V., Ghatkesar M.K., Bredekamp A.H., Gerber C., Hegner M. (2005). Micromechanical mass sensors for biomolecular detection in a physiological environment. *Physical Review E* 72: article 031907.

Datar R., Kim S., Jeon S., Hesketh P., Manalis S., Boisen A., Thundat T. (2009). Cantilever sensors: nanomechanical tools for diagnostics. *MRS Bulletin* 34:449–454.

Fernández-Sáez J., Morassi A., Rubio L., Zaera R. (2019). Transverse free vibration of resonant nanoplate mass sensors: identification of an attached point mass. *International Journal of Mechanical Sciences* 150:217–225.

Gfeller K.Y., Nugaeva N., Hegner M. (2005). Micromechanical oscillators as rapid biosensor for the detection of active growth of Escherichia coli. *Biosensors and Bioelectronics* 21:528–533.

Green A.E. and Rivlin R.S. (1964). Multipolar Continuum Mechanics. *Archive for Rational Mechanics and Analysis* 17:113–147.

Jensen K., Kim K., Zettl A. (2008). An atomic-resolution nanomechanical mass sensor. *Nature Nanotechnology* 3:533–537.

Kong S., Zhou S., Nie Z., Wang K. (2009). Static and dynemic analysis of micro-beams based on strain gradient elasticity theory. *Iternational Journal of Engineering Science* 47:487–498.

Kröner E. (1963). On the physical reality of torque stresses in continuum mechanics. *International Journal of Mechanical Sciences* 1:261–278.

Lam D.C.C., Yang F., Chong A.C.M., Wang J., Tong P. (2003). Experiments and theory in strain gradient elasticity. *Journal of the Mechanics and Physics of Solids* 51:1477–1508.

Lim T.-C. (2011). *Nanosensors: Theory and Applications in Industry, Healthcare and Defense*, First Edition. Boca Raton, FL: CRC Press.

Mindlin R.D. (1964). Micro-structure in linear elasticity. *Archive for Rational Mechanics and Analysis* 16:51–78.

Morassi A., Fernández-Sáez J., Zaera R., Loya J.A. (2017). Resonator-based detection in nanorodas. *Mechanical Systems and Signal Processing* 93:645–660.

Dilena M., Fedele Dell'Oste M., Fernández-Sáez J., Morassi A., Zaera R. (2019). Mass detection in nanobeams from bending resonant frequency shifts. *Mechanical Systems and Signal Processing* 116:261–276.

Romano G., Barretta R., Diaco M., Marotti de Sciarra F. (2017). Constitutive boundary conditions and paradoxes in nonlocal elastic nanobeams. *International Journal of Mechanical Sciences* 121:151–156.

Rubio L., Fernández-Sáez J., Morassi A. (2016).Identification of two cracks with different severity in beams and rods from minimal frequency data. *Journal of Vibration and Control* 22:3102–3117.

Toupin R.A. (1963). Elastic materials with couple-stresses. *Archive for Rational Mechanics and Analysis* 11:385–414.

Voiculescu I., Zaghloul M. (Eds.) (2015). *Nanocantilever Beams. Modeling, Fabrication, and Applications*, First Edition. New York: Taylor & Francis.

Wang Q., Arash B. (2014). A review on applications of carbon nanotubes and graphenes as nano-resonator sensors. *Computational Materials Science* 82: 350-360.